

## Research Paper

# Study the Energy States and Absorption Coefficients of Quantum Dots and Quantum Anti-Dots with Hydrogenic Impurity Under the Applied Magnetic Field

Fatemeh Rahimi<sup>1</sup>, Tooraj Ghaffary\*<sup>1</sup>, Yaghoob Naimi<sup>2</sup>, Hadi Khajehazad<sup>1</sup>

<sup>1</sup>Department of Physics, Faculty of Sciences, Shiraz Branch, Islamic Azad University, Shiraz, Iran

<sup>2</sup>Department of Physics, Lamerd Higher Education Center, Lamerd, Iran

Received: 14 Sep. 2021

Revised: 24 Oct. 2021

Accepted: 23 Nov. 2021

Published: 5 Mar. 2022

Use your device to scan  
and read the article online



### Keywords:

Absorption Coefficient,  
Confinement Potential,  
Degeneracy, Energy States

**Abstract:** In this work, the effect of magnetic field on electronic spectra and absorption coefficient of  $GaAs/Ga_{1-x}Al_xAs$  spherical quantum dot (QD) and  $Ga_{1-x}Al_xAs/GaAs$  spherical quantum anti-dot (QAD) with hydrogenic impurity are reported both theoretically and numerically. The theoretical results which are obtained based on perturbation theory are in agreement with numerical results, which are obtained by using the finite difference method. Using numerical solutions, energy eigenvalues and eigenfunctions of the Schrödinger equation in these structures are obtained. The effects of the magnetic field on  $1s \rightarrow 2p_0$  absorption coefficient and also on  $1s$  and  $2p$  energy levels of the QD and the QAD have been investigated. The wave functions and energies of an electron in these spherical systems, have been studied. The results clearly show that the energy levels changes and absorption coefficients in the QD and QAD models are significantly different. It is also observed some new degeneracies are appeared in the QAD model under the applied magnetic field.

**Citation:** Rahimi F, Ghaffary T, Naimi Y, Khajehazad H. Study the energy states and absorption coefficients of quantum dots and quantum anti-dots with hydrogenic impurity under the applied magnetic field. *Res Sport Sci Med Plants*. 2020; 1 (1): 48- 57. **Journal of Optoelectrical Nanostructures**. 2022; 7 (1): 1- 18. DOI: [10.30495/JOPN.2021.28784.1232](https://doi.org/10.30495/JOPN.2021.28784.1232)

\*Corresponding author: Tooraj Ghaffary

Address: Department of Physics, Faculty of Sciences, Shiraz Branch, Islamic Azad University, Shiraz, Iran. **Tell:** 00989371322746 **Email:** tooraj.gh@gmail.com

## 1. INTRODUCTION

Due to the having an immense potential for device applications, physical properties of low-dimensional semiconductors are widely investigated by many theoretical and experimental researchers. Low dimensional systems in which the motion of the carriers is confined in one, two, and three dimensions are known as quantum wells, quantum wires, and QDs or QADs, respectively [1-9]. Among them QDs and QADs have attracted a great deal of attention on the ground of having tremendous applications in technology [10-18]. Because of the recent improvements in modern fabrication techniques, it is possible to grow these structures with well-controlled dimensions and compositions [19]. The physical properties of these systems can be controllable pursuant to aim by suitable selection of the sample geometry, material parameters, confinement potential, system size and applied external fields, which can generate new usages in optoelectronic devices. The major purpose of the proper selection of the any profile mentioned upper is to manipulate the electronic properties until reaching the best reflect in the material atomic structure and providing the new optoelectronic devices design. Hence, these systems have been greatly researched under the external fields such as electric and magnetic fields and are still being investigated [20-23]. Furthermore, these structures have uncommon and interesting electronic and optical properties like the intersubband optical transitions [24]. On the ground of having these electronic and optical properties, a great number of theoretical studies on the linear and nonlinear optical properties such as absorption coefficient of QD (QAD) nanostructures have been placed in the literature [25-28]

In this work, we have investigated the effect of the magnetic field on the spherical  $GaAs/Ga_{1-x}Al_xAs$  finite QDs and spherical  $Ga_{1-x}Al_xAs/GaAs$  finite QADs energy states theoretically and numerically in such a way that the results are completely consistent. With the comparative view that we had for the QD and QAD models, it was found that these two models have different behavior against changing different parameters such as magnetic field, radius size and confinement potential under the same conditions. They respond differently even to changes in absorption coefficient and in some cases they behave the exact opposite.

The outline of the present paper is as follows: In Sec.2. A brief theoretical background of the systems is given. The numerical results and the corresponding discussions are presented in Sec. 3. Eventually a brief summation is made in sec.4.

## 2. THEORETICAL FRAMEWORK

In the effective mass approximation, the Hamiltonian of an electron in the finite spherical QD and QAD with donor impurity atom located at the center is defined as [29]:

$$H^0 = \frac{\vec{p}^2}{2m^*} + V_C(r) - \frac{e^2 Z}{\epsilon|\vec{r}|} \quad (1)$$

where  $\vec{p}$  is the electron momentum operator,  $m^*$  is the electron effective mass,  $\epsilon$  is the static dielectric constant,  $e$  is the absolute value of electron charge,  $r$  is the electron vector-position with respect to the QD center.  $V_C(r)$  is the finite confinement potential, which are written as Eq. 2 and Eq. 3 for QD and QAD, respectively:

$$V_C^{QD}(r) = \begin{cases} V_0 & r \leq R_1 \\ V_1 & R_1 < R \leq R_2 \\ \infty & \text{otherwise} \end{cases} \quad (2)$$

$$V_C^{QAD}(r) = \begin{cases} V_1 & r \leq R_1 \\ V_0 & R_1 < R \leq R_2 \\ \infty & \text{otherwise} \end{cases} \quad (3)$$

Here  $R_1$  and  $R_2$  are the core and total radii of QD (QAD) and  $V_0$  and  $V_1$  are the values of the potential energy barrier at the boundary of the GaAs sphere and the Ga<sub>1-x</sub>Al<sub>x</sub>As spherical layer (see fig.1) and are defined as follows:

$$\begin{aligned} V_0 &= 0, \\ V_1 &= Q_C 1.247xeV \end{aligned} \quad (4)$$

where  $Q_C$  is the conduction band offset parameter and  $x$  is the Al concentration.

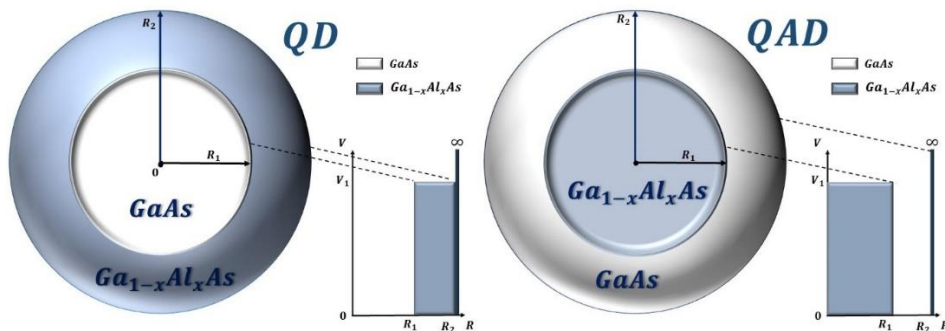


**Fig. 1.** Geometrical and potential energy scheme of QD and QAD models.

Fig. 1 shows an overview of  $GaAs/Ga_{1-x}Al_xAs$  QD and  $Ga_{1-x}Al_xAs/GaAs$  QAD with their potential characteristics where  $R_1$  is the core radius,  $R_2$  is the total radius.

In the presence of the magnetic field the Hamiltonian is given by [30,31]:

$$H = \frac{1}{2m^*} \left( \vec{p} + \frac{e}{c} \vec{A} \right)^2 + V_C(r) - \frac{e^2 Z}{\epsilon |\vec{r}|} \quad (5)$$

where the first term represents the kinetic energy term of the electron in the influence of magnetic field and the vector potential  $\vec{A} = \frac{1}{2} \vec{B} \times \vec{r}$  is associated with the z-axis magnetic field.

Using the effective Rydberg constant  $Ry^* = \frac{m^* e^4}{32\pi^2 \epsilon^2 \hbar^2}$  as the unit of the energy and the effective Bohr radius  $a_0^* = \frac{4\pi\epsilon\hbar^2}{m^* e^2}$  as the unit of the length, Eq. 5 becomes:

$$H = -\nabla^2 - \frac{2}{r} + V_C(r) + m\gamma + \frac{1}{4} \gamma^2 r^2 \sin^2 \theta \quad (6)$$

where  $\gamma = \frac{a_0^{*2} eB}{\hbar c}$ , is the dimensionless parameter depending on magnetic field,  $m$  is the magnetic momentum quantum number and  $\theta$  is considered as the angle between  $r$  and  $z$  axis. The energy levels and their corresponding wave functions can be calculated by solving the following eigenvalue equation:

$$H\psi_{nlm}(r, \theta, \varphi) = E_{nlm}\psi_{nlm}(r, \theta, \varphi) \quad (7)$$

where  $n, l$  are the principal and angular momentum quantum numbers.

Under the applied magnetic field and impurity atom in the systems, there will be no exact solutions to Eq. 7. But according to the perturbation theory, Hamilton in Eq. 6 is divided into two parts:

$$H = H^0 + H^I \quad (8)$$

where  $H^0$  is the unperturbed Hamiltonian of system and it is given by Eq. 9 in which an exact solution can be assumed for it.

$$H^0 = -\nabla^2 - \frac{2}{r} + V_C(r) \quad (9)$$

$H^I$  which is caused by the presence of an external magnetic field is the perturbation Hamiltonian and it is defined as follows:

$$H^I = m\gamma + \frac{1}{4} \gamma^2 r^2 \sin^2 \theta \quad (10)$$

The eigenvalue equation for unperturbed Hamiltonian  $H^0$  is defined as

$$H^0 \psi_{nlm}^{(0)}(r, \theta, \varphi) = E_{nl}^0 \psi_{nlm}^{(0)}(r, \theta, \varphi) \quad (11)$$

Where the  $\psi_{nlm}^{(0)}(r, \theta, \varphi)$  is the normalized wave function of the electron (called the base function) that can be separated into the radial and the angular parts as follows

$$\psi_{nlm}^{(0)}(r, \theta, \varphi) = R_{nl}^{(0)}(r) Y_{lm}(\theta, \varphi) \quad (12)$$

where  $R_{nl}^{(0)}(r)$  and  $Y_{lm}(\theta, \varphi)$  are the radial and the angular part of the unperturbed electron wave function respectively. The radial part of the Eq. 11 can be written as

$$\frac{d^2 R_{nl}^{(0)}(r)}{dr^2} + \frac{2}{r} \frac{dR_{nl}^{(0)}(r)}{dr} - \left[ \frac{l(l+1)}{r^2} - \frac{2}{r} + V_c - E_{nl}^0 \right] R_{nl}^{(0)}(r) = 0 \quad (13)$$

the solution of above equation can be written in the terms of Whittaker functions [32].

$$R_{nl}^{(0)}(r) = N \begin{cases} \xi_1^{-1} M_{\lambda_1, l+\frac{1}{2}}(\xi_1) & \text{region with } V_c = V_1 \\ \xi_2^{-1} W_{\lambda_2, l+\frac{1}{2}}(\xi_2) & \text{region with } V_c = V_0 \\ 0 & \text{region with } V_c = \infty \end{cases} \quad (14)$$

Where  $\alpha_1^2 = -4(E_{nl}^0 - V_1)$ ,  $\alpha_2^2 = -4E_{nl}^0$ ,  $\xi_i = \alpha_i r$ ,  $\lambda_i = 2\alpha_i^{-1}$  and  $N$  is the normalization constant (for more details see [33,34]). The unknown coefficients and energies are obtained by using the boundary conditions of the wave functions and their derivatives at  $r = R$ .

In the following  $|1,0,0\rangle$  and  $|2,1,m\rangle$  with  $m = -1,0,+1$  are considered as the energy wave function of Hamilton  $H^0$  for the  $1s$  and  $2p$  states, respectively. When  $H^0$  is perturbed by the Hamiltonian  $H^1$ , to the first order of the perturbation theory, the  $1s$  and  $2p$  energies will be as follows:

$$E_{1,0,0} = E_{1,0}^0 + \frac{1}{6} \gamma^2 \langle r^2 \rangle_{1,0} \quad (15)$$

$$E_{2,1,m} = \begin{cases} E_{2,1}^0 - \gamma + \frac{1}{5}\gamma^2\langle r^2 \rangle_{2,1}, & m = -1 \\ E_{2,1}^0 + \frac{1}{10}\gamma^2\langle r^2 \rangle_{2,1}, & m = 0 \\ E_{2,1}^0 + \gamma + \frac{1}{5}\gamma^2\langle r^2 \rangle_{2,1}, & m = +1 \end{cases} \quad (16)$$

Where  $E_{1,0}^0$  and  $E_{2,1}^0$  are the energies of  $1s$  and  $2p$  states in the absence of the applied magnetic field and  $\langle r^2 \rangle_{1,0} = \langle 1,0|r^2|1,0 \rangle$  and  $\langle r^2 \rangle_{2,1} = \langle 2,1|r^2|2,1 \rangle$  are the expectation values of  $r^2$  with respect to the spatial part of eigenstates.

As expected, the applied magnetic field removed the triple degeneracy of  $2p$  level and splits the  $2p$  state into three sub-levels ( $2p_{+1}$ ,  $2p_0$  and  $2p_{-1}$ ). By equating the energies of the three sub-levels in Eq. 16, it can be concluded that, except for the value of  $\gamma = 0$ , there is the certain value for  $\gamma$ , (see Eq. 17), in which the energy of the two sub-levels  $2p_0$  and  $2p_{-1}$  will be equal again and this causes the new degeneracy in these two levels. However, the energy of  $2p_{+1}$  level will always be far from the other two levels and will never cross the  $2p_0$  and  $2p_{-1}$  levels and it does not create new degeneracy.

$$\gamma = \gamma_c = \frac{10}{\langle r^2 \rangle_{2,1}} \quad (17)$$

Another conclusion that can be drawn from Eq. 16 is that the energy gap between  $2p_{+1}$  and  $2p_{-1}$  is always equal to  $2\gamma$ , As shown in Eq. 18.

$$\Delta E = E_{2,1,+1} - E_{2,1,-1} = (E_{2,1}^0 + E_{+1}^I) - (E_{2,1}^0 + E_{-1}^I) = 2\gamma \quad (18)$$

Furthermore Eq. 7 can be solved by using of numerical methods such as finite-difference method, too. The numerical values of  $2p$  energies gaps and also the  $\gamma_c$ -values are given in Table 1.

Having the  $1s$  and  $2p$  energies and the corresponding wave functions, it is possible to obtain the optical properties associated with the transition between these two levels. In particular, we are interested in the first-order, third-order and total absorption coefficient.

Using density matrix approach and iterative procedure, under two-level system approximation, the linear  $\alpha^{(1)}(\omega)$  and third-order nonlinear  $\alpha^{(3)}(\omega, I)$  absorption coefficients, in the systems in question are expressed by the following equations [35,36]:

$$\alpha^{(1)}(\omega) = \omega \sqrt{\frac{\mu}{\epsilon_R}} \frac{\sigma_v \hbar \Gamma_{21} |M_{21}|^2}{(E_{21} - \hbar\omega)^2 + (\hbar\Gamma_{21})^2} \quad (19)$$

and

$$\alpha^{(3)}(\omega, I) = -\sqrt{\frac{\mu}{\epsilon_R}} \left( \frac{I}{2\epsilon_0 n_r c} \right) \frac{4\sigma_v \hbar \omega \Gamma_{21} |M_{21}|^4}{[(E_{21} - \hbar\omega)^2 + (\hbar\Gamma_{21})^2]^2} \quad (20)$$

Finally, the total absorption coefficient is calculated from the following equation:

$$\alpha(\omega, I) = \alpha^{(1)}(\omega) + \alpha^{(3)}(\omega, I) \quad (21)$$

where  $M_{21} = |\langle \psi_2 | ez | \psi_1 \rangle|$  is the dipole matrix element for z-polarized incident radiation,  $E_{21} = E_2 - E_1$  is the energy difference between the initial and final states,  $\Gamma_{21} = \frac{1}{T_{21}}$  in which  $T_{21}$  is the relaxing time between initial state and final state.  $\mu$ ,  $\sigma_v$  and  $n_r$  are the permeability, carrier density and refractive index of the system respectively and  $I$  stands for the intensity of the incident field.

### 3. RESULTS AND DISCUSSION

As commented above, in this work the effects of magnetic field on electronic spectra and absorption coefficient of  $GaAs/Ga_{1-x}Al_xAs$  spherical QD and  $Ga_{1-x}Al_xAs/GaAs$  spherical QAD are investigated. The used parameters are  $m^* = 0.067m_0$  ( $m_0$  is the free electron mass),  $\epsilon = 13.18\epsilon_0$ ,  $a_0^* = 10.4nm$ ,  $Ry^* = 5.2meV$ ,  $Q_C = 0.6$ ,  $\Gamma_{21} = 0.2ps$ ,  $\sigma_v = 3 \times 10^{22}$  and  $n_r = 3.2$  [29,34]:

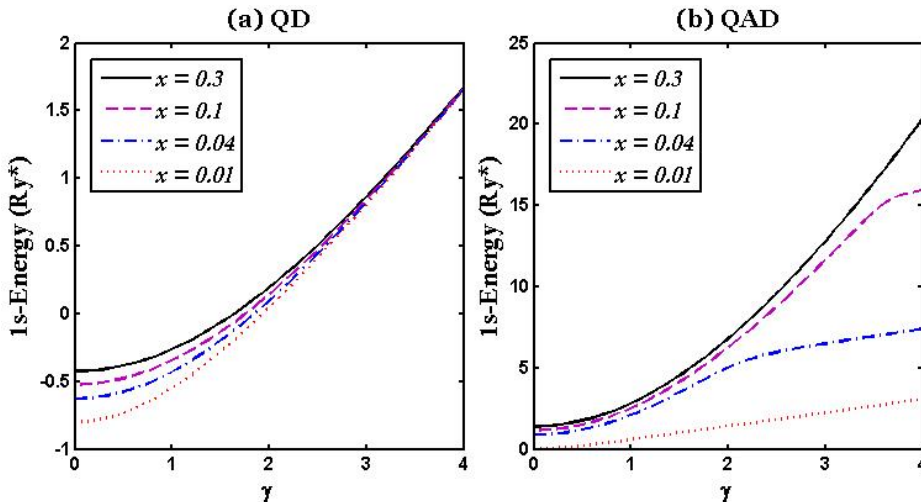


Fig. 2. Variation of 1s energy as a function of  $\gamma$ , for four different values of  $x$ , with  $R_1 = 2a_0^*$  and  $R_2 = 4a_0^*$ .

Fig. 2 illustrate the 1s energy level changes due to the changes in the magnetic field for QD and QAD models for four different values of  $x$  ( $x = 0.3, 0.1, 0.04$  and  $0.01$ ). According to the behavior of the curves in Fig. 2, we find that increasing the magnetic field increases the energy in both models for all  $x$  values. In addition, the graphs clearly show that, as expected, the amount of energy is directly proportional to the value of parameter  $x$ , the concentration of aluminum, which regulates the height of the potential barrier and  $x$  reduction reduces energy in both models. However, the rate of this energy reduction is very different in QD and QAD models.

**TABLE 1**  
**Variations of 2p energies for QD and QAD as function of  $\gamma$  and  $\gamma_c$  values with  $R_1 = 2a_0^*$ ,  $R_2 = 4a_0^*$  and  $x = 0.3$ .**

QD						QAD					
$\gamma$	$2p_{-1}$	$2p_0$	$2p_{+1}$	$\Delta E$	$\gamma_c$	$\gamma$	$2p_{-1}$	$2p_0$	$2p_{+1}$	$\Delta E$	$\gamma_c$
0	2.571 3	2.57 13	2.571 3	0	6.116 0	0	1.6493 3	1.649 3	1.649 3	0	1.15 11
1	1.894 7	2.73 39	3.894 7	2	6.184 6	1	2.3536 7	2.509 6	4.353 6	2	1.17 36
2	1.822 4	3.21 10	5.822 4	4	6.396 2	2	6.1029 0	4.994 29	10.10 29	4	1.24 23
3	2.236 0	3.97 10	8.236 0	6	6.767 6	3	12.132 2	8.848 5	18.13 22	6	1.35 15
4	2.974 4	4.96 57	10.97 44	8	7.319 7	4	19.942 2	13.79 15	27.94 22	8	1.47 68

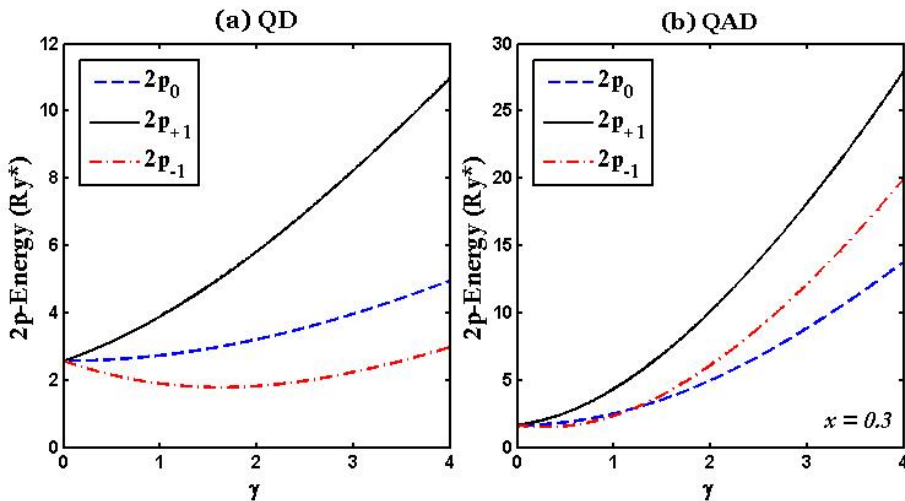
(Energies are presented in  $Ry^*$ )

Table 1 and Table 2 show the changes in 2p energies and the values of  $\gamma_c$  in the range of changes  $0 \leq \gamma \leq 4$  which are obtained by our numerical calculations for  $x = 0.3$  and  $x = 0.04$ , respectively. As can be seen the results are quite consistent with the theoretical achievements found in the theory sections. These two Tables show that, as predicted in Eq. 18, we have for both models:  $\Delta E = E_{2,1,+1} - E_{2,1,-1} = 2\gamma$ .

**TABLE 2**  
 Variations of  $2p$  energies for QD and QAD as function of  $\gamma$  and  $\gamma_c$  values with  $R_1 = 2a_0^*$ ,  $R_2 = 4a_0^*$  and  $x = 0.04$ .

QD						QAD					
$\gamma$	$2p_{-1}$	$2p_0$	$2p_{+1}$	$\Delta E$	$\gamma_c$	$\gamma$	$2p_{-1}$	$2p_0$	$2p_{+1}$	$\Delta E$	$\gamma_c$
0	1.795	1.795	1.795	0	4.46	0	1.181	1.181	1.181	0	1.281
	5	5	5		60		6	6	6		6
1	1.228	2.015	3.228	2	4.61	1	1.682	1.947	3.682	2	1.332
	8	6	8		89		5	0	5		5
2	1.392	2.636	5.392	4	5.03	2	4.459	4.063	8.459	4	1.516
	9	9	9		69		5	1	5		8
3	2.023	3.571	8.023	6	5.67	3	7.187	6.979	13.18	6	1.985
	7	1	7		18		0	8	70		1
4	2.892	4.721	10.89	8	6.50	4	8.537	6.676	16.53	8	3.605
	5	7	25		79		3	9	73		8

(Energies are presented in  $Ry^*$ )



**Fig. 3.** Variation of  $2p$  energies as a function of  $\gamma$  with  $R_1 = 2a_0^*$ ,  $R_2 = 4a_0^*$  and  $x = 0.3$ .

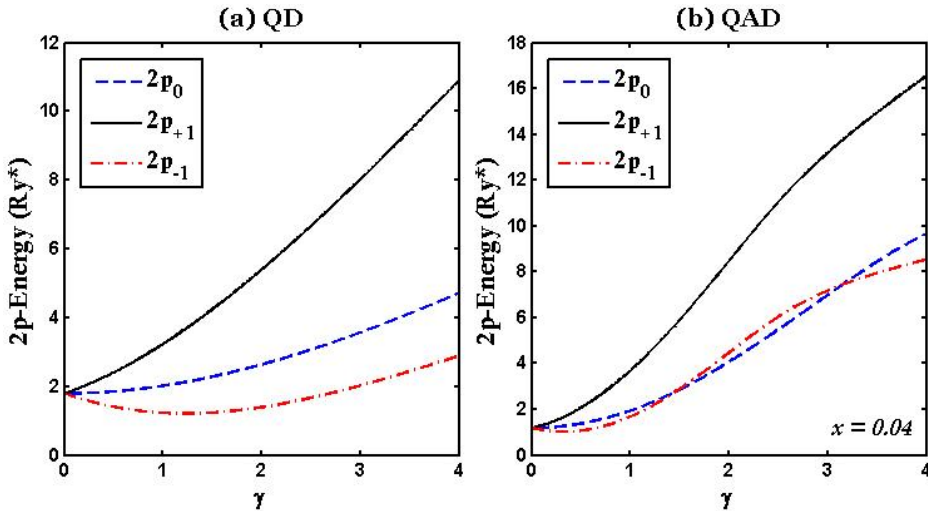


**Fig. 4.** Variation of  $2p$  energies as a function of  $\gamma$  with  $R_1 = 2a_0^*$ ,  $R_2 = 4a_0^*$  and  $x = 0.04$ .

In Fig. 3 and Fig. 4 the  $2p$  energy states for (a) QD and (b) QAD as a function of  $\gamma$  with constant values of core radius  $R_1 = 2a_0^*$  and total radius  $R_2 = 4a_0^*$  for  $x = 0.3$  and  $x = 0.04$ , are depicted respectively. It can be observed, in the case of  $2p$  level, as expected, the applied magnetic field causes this level to split into three sub-levels ( $2p_{-1}, 2p_0, 2p_{+1}$ ) and the triple degeneracy of this level is completely removed. The interesting and remarkable point about the separation of  $2p$  levels under the applied magnetic field is that for the certain values of  $\gamma$  in Fig. 3(b) and Fig. 4(b) the  $2p_{-1}$  and  $2p_0$  curves cross each other. These intersection points indicate the new degeneracies in the presence of the magnetic field. We had predicted these new degeneracies in the presence of the magnetic field for  $2p$  level in the theoretical part, (Sec. 2), and the numerical values of our prediction for  $\gamma_c$  are given in Table 1 and Table 2 for  $x = 0.3$  and  $x = 0.04$ , respectively. It can be seen in Table 1 that when  $0 \leq \gamma \leq 4$  then for QD model  $6.1160 \leq \gamma_c \leq 7.3197$  and for QAD model  $1.1511 \leq \gamma_c \leq 1.4768$ . As one can see in QD model, the  $\gamma_c$  range is not in  $\gamma$  range, hence the  $2p$  curves of this model do not intersect each other and  $2p$  energy states will not become degenerate again in QD model. But in QAD model, the  $\gamma_c$  range is completely in  $\gamma$  range, and this causes the  $2p_{-1}$  and  $2p_0$  curves to intersect at a point between  $\gamma = 1.1115$  and  $\gamma = 1.4768$ , and create a new degeneracy. As the value of  $x$  decreases from 0.3 to 0.04 in Fig. 4, the number of intersection points increases to two points in QAD model, but QD curves remain without any intersection point. In this case, Table 2 shows that when  $0 \leq \gamma \leq 4$  then for QD

model  $4.4660 \leq \gamma_C \leq 6.5079$  and for QAD model  $1.2816 \leq \gamma_C \leq 3.6058$ . And again, it is observed that due to the lack of overlap of  $\gamma$  and  $\gamma_C$  ranges in QD model, new degeneracy will not appeared, but due to the overlap in  $\gamma$  and  $\gamma_C$  ranges in QAD model, in the range predicted in Table 2, there are two degeneracies between  $2p_0$  and  $2p_{-1}$  levels. Furthermore, by comparing Figs. 3 and 4, It is found that  $x$  reduction, reduces  $2p$  energy levels in both models.

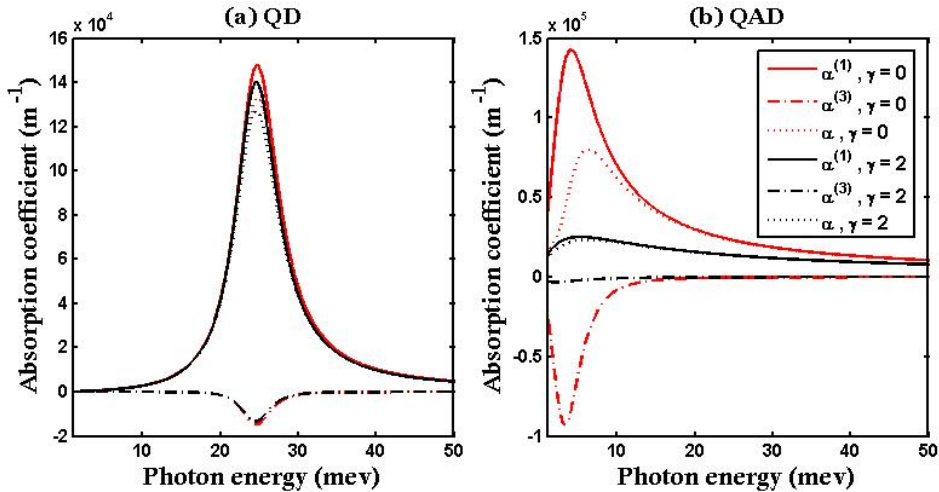


**Fig. 5.** The linear, nonlinear and total absorption coefficient as a function of incident photon energy in the presence and absence of the applied magnetic field with  $I = 200\text{MW}/\text{m}^2$ ,  $R_1 = 1.5a_0^*$ ,  $R_2 = 3a_0^*$ ,  $x = 0.3$ .

The changes in the linear, nonlinear and total  $1s \rightarrow 2p_0$  absorption coefficient as a function of incident photon energy for two values of  $\gamma$  (0 and 2) are noticeable in Fig. 5 (a) QD and (b) QAD. Fig. 5 shows that the presence of a magnetic field reduces the absorption coefficients in both models. Furthermore, carefully in Fig. 5, the following differences are understood between QD and QAD models: i) the QD model has an almost symmetric total absorption coefficient curve while Fig. 2 (b) shows no symmetry in QAD total absorption coefficient curve. ii) For the same value of intensity, QAD model has a more significant nonlinear absorption coefficient diagram than QD model. Therefore according to the Eq. 19 to Eq. 21 it can be concluded that the total absorption coefficient in QAD model is much more sensitive to intensity changes than QD model. iii) The changes in the applied magnetic field in the displacement of the absorption coefficient curves in QAD model are much stronger than in QD model, and QAD model clearly responds more severe to the magnetic field.

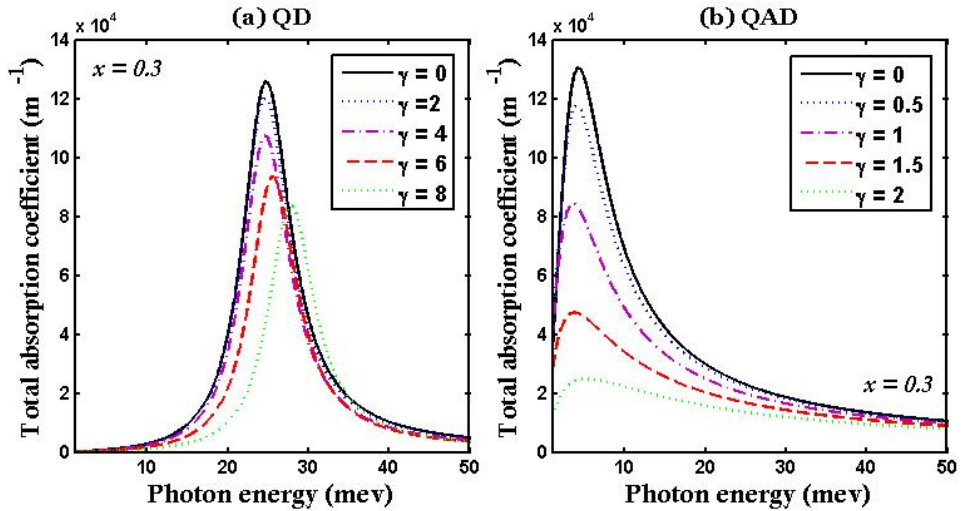


Fig. 6. Variation of total absorption coefficient as a function of incident photon energy for different values of  $\gamma$  with  $I = 300\text{MW}/\text{m}^2$  for the QD and  $I = 30\text{MW}/\text{m}^2$  for the QAD and  $R_1 = 1.5a_0^*$ ,  $R_2 = 3a_0^*$ ,  $x=0.3$ .

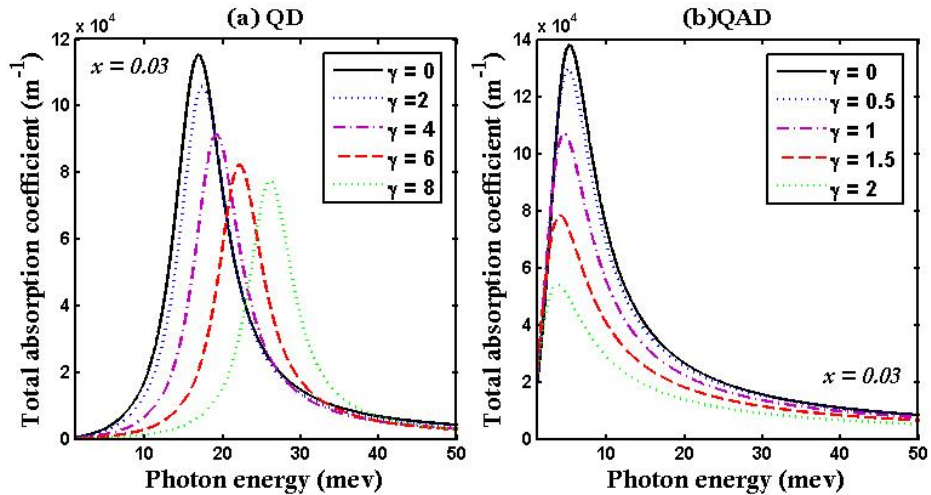


Fig. 7. Variation of total absorption coefficient as a function of incident photon energy for different values of  $\gamma$  with  $I = 300\text{MW}/\text{m}^2$  for the QD and  $I = 30\text{MW}/\text{m}^2$  for the QAD and  $R_1 = 1.5a_0^*$ ,  $R_2 = 3a_0^*$ ,  $x=0.03$ .

Fig. 6 and Fig. 7 the variation of total absorption coefficient are plotted under the same conditions with only one difference. In Fig. 6, the concentration of aluminum, which regulates the height of the potential barrier, is selected  $x=0.3$ ,

while in Fig. 7 this value is reduced to 0.03. In order to investigate the effect of magnetic field on the  $1s \rightarrow 2p_0$  total absorption coefficient of (a) QD with  $I = 300 \text{ MW/m}^2$  and (b) QAD with  $I = 30 \text{ MW/m}^2$ , the changes in the total absorption coefficient are plotted with respect to changes in the incident photon energy for five different  $\gamma$  values in Fig. 6 and Fig. 7. For the reasons stated in the descriptions of Fig. 5, the magnitude of the intensity as well as the range of the magnetic field in Fig. 6,7(a) and Fig. 6,7(b) have been chosen differently. These Figures clearly show that increasing the magnetic field reduces the absorption coefficient in both models and in QD model the peaks shift to greater incident photon energy. The reasons for these behaviors are that as the  $\gamma$  increases, the energy difference between the two electron states increases and the overlap of wave functions and as a result the total absorption coefficient has decreased. Furthermore, in QD model, increasing the energy difference between the initial and final energy levels by increasing the  $\gamma$ , has caused the peaks of the absorption coefficient shift towards greater incident photon energy.

Closer look at Fig. 6 and 7 can give the conclusion that with decreasing the concentration of aluminum, the sensitivity to the magnetic field has increased (decreased) in QD (QAD) model. Comparison of Fig. 6(a) and Fig. 7(a) shows that when  $x$  decreases from 0.3 to 0.03, the absorption coefficient peaks have larger shifts towards the greater photon energy in QD model and this shows that with decreasing  $x$ , the sensitivity of this model to magnetic field has increased. But in QAD model when  $x$  decreases from 0.3 to 0.03, the rate of absorption coefficient changes with the changes of the magnetic field, decreases and this indicates that the sensitivity of QAD model has decreased.

#### 4. CONCLUSION

In this paper, the effects of the magnetic field on  $1s \rightarrow 2p_0$  absorption coefficient and also on  $1s$  and  $2p$  energy levels of spherical  $GaAs/Ga_{1-x}Al_xAs$  finite QD and spherical  $Ga_{1-x}Al_xAs/GaAs$  finite QAD with hydrogenic impurity have been investigated. The wave functions and energies of an electron in these spherical systems, have been studied. Our results in the framework of the effective mass approximation show that there are some critical values  $\gamma_C$  for the magnetic field in which the energy levels of  $2p_0$  and  $2p_{-1}$  become degenerate again in the QAD. This phenomenon which was anticipated in our theoretical methods can be seen from our numerical calculations too. Furthermore, the  $1s \rightarrow 2p_0$  absorption coefficients of the QD and the QAD have different operation relative to the incident photon energies for different values of  $\gamma$ .

## REFERENCES

- [1] Y. Liu, H. Xie, Y. Xing, *Optical vibration modes in multi-layer quantum dots of polar ternary mixed crystals*, Physica E, 121 (2020) 114124. Available: <https://doi.org/10.1016/j.physe.2020.114124>
- [2] A. Ghadimi, M. Ahmadzadeh, *Effect of Variation of Specifications of Quantum Well and Contact Length on Performance of Inp-Based Vertical Cavity Surface Emitting Laser (VCSEL)*, Journal of Optoelectrical Nanostructures, 5(1) (2020) 19–34. Available: [http://jopn.miau.ac.ir/article\\_4031.html](http://jopn.miau.ac.ir/article_4031.html)
- [3] E. Kasapoglu, H. Sari, I. Sökmen, J.A. Vinasco, D. Laroze, C.A. Duque, *Effects of intense laser field and position dependent effective mass in Razavy quantum wells and quantum dots*, Physica E, 126 (2021) 114461. Available: <https://doi.org/10.1016/j.physe.2020.114461>
- [4] M. Servatkah, *Study of RbCl quantum pseudo-dot qubits using Shannon and Laplace entropies*, Optical and Quantum Electronics, 52 (2020) 126. Available: <https://doi.org/10.1007/s11082-020-2229-6>
- [5] F. Rahimi, T. Ghaffary, Y. Naimi, H. Khajehazad, *Efect of magnetic feld on energy states and optical properties of quantum dots and quantum antidots*, Optical and Quantum Electronics, 53(47) (2021) 1–16. Available: <https://doi.org/10.1007/s11082-020-02695-w>
- [6] R. Betancourt-Riera, R. Betancourt-Riera, L.A. Ferrer-Moreno, A.D. Sañu-Ginarte, *Theory of electron Raman scattering in a semiconductor core/shell quantum well wire*, Physica B, 563 (2019) 93–100. Available: <https://doi.org/10.1016/j.physb.2019.04.004>
- [7] Y. Naimi, J. Vahedi, M. R. Soltani, *Effect of position-dependent effective mass on optical properties of spherical nanostructures*, Optical and Quantum Electronics, 47 (2015) 2947-2956. Available: <https://doi.org/10.1007/s11082-015-0183-5>

- [8] R. Yahyazadeh, Z. Hashempour, *Numerical Modeling of Electronic and Electrical Characteristics of  $Al_{0.3}Ga_{0.7}N/GaN$  Multiple Quantum Well Solar Cells*, Journal of Optoelectrical Nanostructures, 5(3) (2020) 81–101. Available: [http://jopn.miau.ac.ir/article\\_4406.html](http://jopn.miau.ac.ir/article_4406.html)
- [9] H. Bahramiyan, M. Servatkah, *Second and third harmonic generation of a hexagonal pyramid quantum dot: impurity position effect*, Optical and Quantum Electronics, 47 (2015) 2747-2758.  
Available: <https://doi.org/10.1007/s11082-015-0176-4>
- [10] S. Chaudhuri, *Two-electron quantum dot in a magnetic field: Analytic solution for finite potential model*, Physica E, 128 (2021) 114571.  
Available: <https://doi.org/10.1016/j.physe.2020.114571>
- [11] Y. Naimi, *Refractive index changes of a donor impurity in spherical nanostructures: Effects of hydrostatic pressure and temperature*, Phys. B, 428 (2013) 43–47.  
Available: <https://doi.org/10.1016/j.physb.2013.07.019>
- [12] H. Bahramiyan, S. Bagheri, *Linear and nonlinear optical properties of a modified Gaussian quantum dot: pressure, temperature and impurity effect*, journal of optoelectrical nanostructures, 3 (3) (2018) 79-100.  
Available: <https://www.sid.ir/en/Journal/ViewPaper.aspx?ID=613953>
- [13] L. Stevanović, N. Filipović, V. Pavlović, *Effect of magnetic field on absorption coefficients, refractive index changes and group index of spherical quantum dot with hydrogenic impurity*, Journal of Luminescence, Optical Materials, 91 (2019) 62–69.  
Available: <https://doi.org/10.1016/j.optmat.2019.02.049>
- [14] F. Rahimi, T. Ghaffary, Y. Naimi, H. Khajehazad, *Study of the Spin-Orbit Interaction Effects on Energy Levels and the Absorption Coefficients of Spherical Quantum Dot and Quantum Anti-Dot under the Magnetic Field*, journal of optoelectrical nanostructures, 6 (2) (2021) 55-74.  
Available: <https://doi.org/10.30495/JOPN.2021.27965.1222>
- [15] M. Rezvani Jalal, M. Habibi, *Simulation of Direct Pumping of Quantum Dots in a Quantum Dot Laser*, journal of optoelectrical nanostructures, 2 (2) (2017) 61-69.

Available: <https://www.sid.ir/en/journal/ViewPaper.aspx?id=550467>

- [16] S. Sakiroglu, D. Gul Kilic, U. Yesilgul, F. Ungan, E. Kasapoglu, H. Sari, I. Sokmen, *Intense laser field effects on the third-harmonic generation in a quantum pseudodot system*, Physica B, 521 (2017) 215–220.  
Available: <https://doi.org/10.1016/j.physb.2017.06.071>
- [17] F. Hakimian, M.R. Shayesteh, M.R. Moslemi, *Proposal for Modeling of FWM Efficiency of QD-SOA Based on the Pump/Probe Measurement Technique*, journal of optoelectrical nanostructures, 5 (4) (2020) 49-65.  
Available: [http://jopen.miau.ac.ir/article\\_4509.html](http://jopen.miau.ac.ir/article_4509.html)
- [18] R. Khordad, M. Servatkah, *Study of entanglement entropy and exchange coupling in two-electron coupled quantum dots*, Optical and Quantum Electronics, 49 (2017) 217.  
Available: <https://doi.org/10.1007/s11082-017-1044-1>
- [19] I. Karabulut, H. S. Şafak, M. Tomak, *Excitonic effects on the nonlinear optical properties of small quantum dots*, J. Phys. D: Appl. Phys, 41 (2008) 155104.  
Available: <https://doi.org/10.1088/0022-3727/41/15/155104>
- [20] G.V.B. de Souza, A. Bruno-Alfonso, *Finite-difference calculation of donor energy levels in a spherical quantum dot subject to a magnetic field*, Physica E, 66 (2015) 128–132.  
Available: <https://doi.org/10.1016/j.physe.2014.10.011>
- [21] M. Jaouane, A. Sali, A. Ezzarfi, A. Fakkahi, R. Arraoui, *Study of hydrostatic pressure, electric and magnetic fields effects on the donor binding energy in multilayer cylindrical quantum dots*, Physica E, 127 (2021) 114543.  
Available: <https://doi.org/10.1016/j.physe.2020.114543>
- [22] K.L. Jahan, A. Boda, I.V. Shankar, Ch. N. Raju, A. Chatterjee, *Magnetic field effect on the energy levels of an exciton in a GaAs quantum dot: Application for excitonic lasers*, Sci Rep, 8 (2018) 5073.  
Available: <https://doi.org/10.1038/s41598-018-23348-9>

- [23] S. M. Bilankohi, M. Ebrahimzadeh, T. Ghaffary, *Study of the properties of Au/Ag core/shell nanoparticles and its application*, Indian Journal of Science and Technology, 8 (2015) 31-33.  
Available: <https://doi.org/10.17485/ijst/2015/v8iS9/68667>
- [24] K. Khordad, *Temperature effect on the threshold frequency of absorption in a quantum pseudodot*, Physica, B 406 (2011) 620-623.  
Available: <https://doi.org/10.1016/j.physb.2010.11.059>
- [25] M. Choubani, R.B. Mahrsia, L. Bouzaiene, H. Maaref, *Nonlinear optical rectification in vertically coupled InAs/GaAs quantum dots under electromagnetic fields, pressure and temperature effects*, J. Luminesc, 144 (2013) 158-162.  
Available: <https://doi.org/10.1016/j.jlumin.2013.07.002>
- [26] H. Khajehazad, T. Ghaffary, M. Ebrahimzadeh, *Microwave Absorption Properties of Fe<sub>2</sub>O<sub>3</sub>/Paraffin Wax Nanocomposite*, Asian J. Chem., 25(13) 7651-7652, (2013).  
Available: <https://doi.org/10.14233/ajchem.2013.15155>
- [27] F. Rahmani, J. Hasanzadeh, *Investigation of the Third-Order Nonlinear Optical Susceptibilities and Nonlinear Refractive Index In Pbs/Cdse/Cds Spherical Quantum Dot*, journal of optoelectronical nanostructures, 3 (1) (2018) 65-78.  
Available: [http://jopn.miau.ac.ir/article\\_2824.html](http://jopn.miau.ac.ir/article_2824.html)
- [28] X.F. Yan, Q. Chen, W. Pei, J.Z. Peng, *Magnetic field dependence of the electronic and optical properties of silicene quantum dots*, Solid State Communications, 327 (2021) 114219.  
Available: <https://doi.org/10.1016/j.ssc.2021.114219>
- [29] Y. Naimi, A.R. Jafari, *Optical properties of quantum dots versus quantum antidots: Effects of hydrostatic pressure and temperature*, Journal of Computational Electronics, 13 (2014) 666-672.  
Available: <https://doi.org/10.1007/s10825-014-0585-9>
- [30] E.B. Al, E. Kasapoglu, S. Sakiroglu, H. Sari, I. Sokmen, C.A. Duque, *Binding energies and optical absorption of donor impurities in spherical quantum dot under applied magnetic field*, Physica E, 119 (2020) 114011.

Available:<https://doi.org/10.1016/j.physe.2020.114011>

- [31] B. Çakır, Y. Yakar, A. Özmen, *Investigation of Magnetic Field Effects on Binding Energies in Spherical Quantum Dot with Finite Confinement Potential*, Chemical Physics Letters, 684 (2017) 250–256.  
Available:<https://doi.org/10.1016/j.cplett.2017.06.064>
- [32] A. Abramowitz, I. Stegun, *Handbook of Mathematical Function with Formulas Graphs and Mathematical Tables*, (1964), pp. 505–509. US GPO, Washington, D.C.
- [33] Y. Naimi, A.R. Jafari, *Oscillator strengths of the intersubband electronic transitions in the multi-layered nano-antidots with hydrogenic impurity*, J. Comput. Electron, 11(2012) 414-420.  
Available:<https://doi.org/10.1007/s10825-012-0421-z>
- [34] A.R. Jafari, Y. Naimi, *Linear and nonlinear optical properties of multi-layered spherical nano-systems with donor impurity in the center*, J. Comput. Electron, 12 (2013) 36-42.  
Available:<https://doi.org/10.1007/s10825-013-0432-4>
- [35] S. M. Bilankohi, M. Ebrahimzadeh, T. Ghaffary, M. Zeidiyam, *Scattering, Absorption and Extinction Properties of Al/TiO<sub>2</sub> Core/Shell Nanospheres*, Indian Journal of Science and Technology, 8 (2015) 1-4  
Available:<https://doi.org/10.17485/ijst/2015/v8iS9/68665>
- [36] M. Servatkah, R. Pourmand, *Optical properties of a two-dimensional GaAs quantum dot under strain and magnetic field*, The European Physical Journal Plus, 135 (2020) 754.  
Available:<https://doi.org/10.1140/epjp/s13360-020-00773-2>